Title

Aptamer-field-effect transistors overcome Debye length limitations for small-molecule sensing.

Journal

Science (New York, N.Y.), 362(6412)

ISSN

0036-8075

Authors

Nakatsuka, Nako
Yang, Kyung-Ae
Abendroth, John M
et al.

Publication Date

2018-10-01

DOI

10.1126/science.aao6750

Peer reviewed

HHS Public Access

Author manuscript

Science. Author manuscript; available in PMC 2019 July 29.

Published in final edited form as:

Science. 2018 October 19; 362(6412): 319–324. doi:10.1126/science.aao6750.

Aptamer-field-effect transistors overcome Debye length limitations for small-molecule sensing

Nako Nakatsuka[1,2], **Kyung-Ae Yang**[3], **John M. Abendroth**[1,2], **Kevin Cheung**[1,2], **Xiaobin Xu**[1,2], **Hongyan Yang**[4], **Chuanzhen Zhao**[1,2], **Bowen Zhu**[1,5], **You Seung Rim**[1,5], **Yang Yang**[1,5], **Paul S. Weiss**[1,2,5,*], **Milan N. Stojanović**[3,6,*], **Anne M. Andrews**[1,2,4,*]

[1]California NanoSystems Institute, University of California, Los Angeles, Los Angeles, CA 90095, United States

[2]Department of Chemistry and Biochemistry, University of California, Los Angeles, Los Angeles, CA 90095, United States

[3]Center for Innovative Diagnostic and Therapeutic Approaches, Department of Medicine, Columbia University, New York, New York 10032, United States

[4]Department of Psychiatry and Biobehavioral Science, Semel Institute for Neuroscience and Human Behavior, and Hatos Center for Neuropharmacology, University of California, Los Angeles, Los Angeles, CA 90095, United States

[5]Department of Materials Science and Engineering, University of California, Los Angeles, Los Angeles, CA 90095, United States

[6]Departments of Biomedical Engineering and Systems Biology, Columbia University, New York, New York 10032, United States

Abstract

Detection of analytes with field-effect transistors bearing ligand-specific receptors is fundamentally limited by the shielding created by the electrical double layer (the “Debye length” limitation). We detected small molecules under physiological high ionic-strength conditions by modifying printed ultrathin metal-oxide field-effect transistor arrays with deoxyribonucleotide aptamers selected to bind their targets adaptively. Target-induced conformational changes of negatively charged aptamer phosphodiester backbones in close proximity to semiconductor channels gated conductance in physiological buffers, resulting in highly sensitive detection. Sensing of charged and electroneutral targets (serotonin, dopamine, glucose, and sphinghosine-1-phosphate) was enabled by specifically isolated aptameric stem-loop receptors.

*Correspondence to: aandrews@mednet.ucla.edu (AMA), mns18@cumc.columbia.edu (MNS), psw@cnsi.ucla.edu (PSW).

Authors conbributions: N.N., K.A.Y., P.S.W., M.N.S., and A.M.A. conceived experiments. N.N. and K.M.C. performed aptamer-FET measurements. K.A.Y. and M.N.S. designed and isolated stem-loop aptamer receptors and conducted FRET measurements. N.N., J.M.A., and X.X. conducted spectroscopy experiments. H.Y. carried out mouse experiments. C.Z., B.Z., Y.S.R., and Y.Y. designed and fabricated thin-film transistors. N.N., P.S.W., M.N.S, and A.M.A. wrote the manuscript.

Competing interests: N.N., K.A.Y, P.S.W, M.N.S., and A.M.A. filed a patent on stem-loop receptor-based field effect sensor devices for sensing at physiological salt concentrations, U.S. application no. 504901225. M.N.S. has patent applications, a start-up company, and consulting income for work on small-molecule aptamers

Data and materials availability: All data needed to evaluate the conclusions in the paper are presented in the paper or the Supplementary Materials.

One Sentence Summary:

Field-effect transistors bearing aptameric stem-loop receptors designed to be conformationally flexible close to semiconductor surfaces detect small-molecule targets under physiological conditions overcoming Debye length limitations.

Field-effect transistors (FETs) modified with target-specific receptors could enable direct electronic target detection (1, 2). Signal transduction and amplification in FET-based sensors is based on electrostatic gating of thin-film semiconductor channels by target-receptor interactions such that even low receptor occupancy measurably affects transconductance (3). However, receptor-modified FETs must overcome two fundamental limitations to be more widely adopted. First, the electrical double layer in solutions containing ions shields semiconductor charge carriers to limit gating in response to recognition events. The extent of shielding, i.e., the effective sensing distance, is characterized by the Debye length, which in physiological fluids is <1 nm (table S1) (4). Second, small target molecules with few or no charges have minimal impact on semiconductor transconductance unless they trigger conformational changes in charged receptors within or near the Debye length, or otherwise affect surface potentials (5).

We overcame both of these obstacles by combining highly sensitive FETs with a specific type of oligonucleotide stem-loop receptor selected for adaptive target recognition (Fig. 1A). We fabricated nanometer-thin In_2O_3 FETs (Fig. 1B) using methods that facilitate micro- and nanoscale patterning and are readily scalable for producing large numbers of devices (2, 6). Sensing with FETs is inherently nonlinear (5), which enables target detection over larger and lower concentration ranges compared to equilibrium-based sensors (7). Although aptamers have been used as receptors for FET devices (2, 8), it proved critical to combine ligand-induced stem-loop conformational rearrangements and close proximity to the surfaces of quasi-two-dimensional FETs. Changes in conformation of negatively charged phosphodiester backbones enabled signal transduction and amplification under biologically relevant conditions with low-charge and neutral targets.

Solution-phase selection of aptamers circumvented tethering small-molecule targets and was based on stem-loop closing with appropriate counterselection against interferents (Fig. 1C) (9, 10). This approach yielded aptamers characterized by adaptive-loop binding. Strategies and details of the selections and counterselections are given in the supplementary material (tables S2,S3, fig. S1). We isolated original receptors for dopamine, serotonin, glucose, and sphingosine-1-phosphate (S1P) (Fig. 1, D to G, table S4). Dopamine was targeted because we had constructed FET devices using a previously reported dopamine aptamer (11) but these required dilute ion concentrations for sensing (2). Serotonin was pursued as another important neurotransmitter target (12) having no reported aptamer sequences. Ultimately, we aim to distinguish serotonin from dopamine and other similarly structured molecules in measurements of interneuronal signaling (13–15). Glucose was selected as an example of an important neutral target. Aptamers interacting directly with glucose have not been reported (although *cf.* aptamers for glucose sensors) (10). The lipid S1P (critical micellar concentration <10 μM), which prevents chemotherapy-associated apoptosis (16), was chosen as an example of a zwitterionic target.

Fluorescence assays were used to characterize aptamer-target dissociation constants (K_d) (fig. S2A). Selection led to high-affinity aptamers for dopamine (150 nM) and serotonin (30 nM) (fig. S2, B and C). Counterselection eliminated interactions with other neurotransmitters and metabolites (Fig. 1, H and I) critical for sensing in the presence of high concentrations of similarly structured countertargets in vivo. Notably, our dopamine aptamer did not recognize norepinephrine, in contrast to cross-reactivity of a previously reported dopamine aptamer (2, 11). Poor selectivity has also been problematic for fast-scan cyclic voltammetry, the most common method for sensing dopamine (13, 17). The affinity of the glucose aptamer (~10 mM) (fig. S2D) and selectivity with respect to analogs (Fig. 1J, fig. S3) were consistent with the receptor recognizing hydrophobic surfaces of glucose (18). The affinity of the S1P aptamer was 180 nM (Fig. 1K, fig. S2E), which was not as high as a reported spiegelmer (4 nM) (19).

We covalently modified thin-film In_2O_3 FETs with dopamine or serotonin aptamers using silane chemistry (fig. S4) to investigate electronic small-molecule detection (Fig. 1A). Despite subnanometer Debye screening lengths, aptamer-FETs responded to wide ranges of target concentrations (10^{-14} to 10^{-9} M) in undiluted, i.e., physiological, phosphate-buffered saline (PBS) (Fig. 2A, fig. S5A) or artificial cerebrospinal fluid (aCSF) (Fig. 2, B and C) with response times on the order of seconds (fig. S6). Scrambled aptamer sequences (table S5) produced negligible responses (Fig. 2, A and C, fig. S5A), as did FETs lacking aptamers (fig. S5, B and C). Even at physiological ion concentrations and hence, substantially reduced Debye lengths, FET responses for our dopamine aptamer were more than three orders of magnitude greater than those of the previously reported dopamine aptamer (11) in PBS diluted tenfold (Fig. 2A) due to designed positioning of recognition regions capable of adaptive conformational changes in the new aptamer.

Dopamine-aptamer-FETs were selective for dopamine vs. serotonin, norepinephrine, tyramine, and dopamine metabolites (Fig. 2D, fig. S6A). Serotonin-aptamer-FETs were selective for serotonin vs. dopamine, norepinephrine, histamine, other biogenic amines, and indole metabolites (Fig. 2E, fig. S6B). Aptamer-FET selectivity was further investigated with surface-enhanced Raman spectroscopy (SERS; fig. S7, A and B). Raman signatures were enhanced only in close proximity to metal surfaces because of the short range of evanescent fields, with the strongest enhancement within ~1 nm of surfaces (similar to the physiological Debye length) (20). After dopamine or serotonin were introduced, SERS spectra exhibited complex pattern changes that were not evident with nontarget compounds (fig. S7, C and D).

To evaluate sensing in an undiluted biological matrix, serotonin was added to brain tissue from mice lacking neuronal serotonin, i.e., *Tph2* null mice (Fig. 2F) (21). Electronic FET responses differentiated physiologically relevant serotonin concentrations (10 pM to 100 nM) (14). Sensor responses to dopamine or the serotonin metabolite, 5-hydroxyindoleacetic acid in tissue were negligible (fig. S8A). The high sensitivity of aptamer-FETs offsets losses often encountered in biological environments and sensitivity for modest changes in target concentrations was observed despite large sensing ranges. Concentration sensitivity ranges could be “tuned” by altering the numbers of serotonin aptamers on FET surfaces (Fig. 2F). Sensor performance in tissue was reproducible when repeated 12 hours later (fig. S8B).

Moreover, continuous exposure of serotonin-aptamer FETs to brain tissue for 1 to 4 hours produced stable concentration-dependent conductance responses and was another indication of sensor stability (Fig. 2G).

Aptamer-FET responses to the zwitterionic lipid S1P were recorded at concentrations ranging from 10 pM to 100 nM. A nontarget lipid (1-myristoyl-2-hydroxy-*sn*-glycero-3-phosphoethanolamine) bearing similar epitopes (Fig. 2H) exhibited negligible responses, as did a scrambled S1P sequence (table S5). Glucose-aptamer-FETs exhibited concentration-dependent responses to glucose (10 pM to 10 nM). The FET responses to other monosaccharides, e.g., galactose and fructose, were minimal, as were responses when a scrambled glucose sequence was used (Fig. 2I; table S5). Experiments with SERS corroborated target-specific recognition in close proximity to substrates for S1P and glucose aptamers (fig. S7, E and F).

We detected glucose in whole blood diluted with Ringer's buffer (10 μM to 1 mM; Fig. 2J). We also measured glucose levels in diluted serum from mice lacking serotonin transporter expression characterized by hyperglycemia (22). Elevations in serum glucose in basal and glucose-challenged states were observed using glucose-aptamer-FETs (Fig. 2K); glucose concentrations were similar to those determined in whole blood using a glucometer (fig. S9). These findings demonstrated the feasibility of aptamer-FET sensing in diluted yet full ionic strength blood/serum and the ability to differentiate modest yet physiologically relevant differences in neutral target concentrations.

Aptamer-FET sensing enabled observations suggestive of mechanism. In addition to FET responses at subthreshold-regime gate voltages (Fig. 2), we examined characteristics of FET transfer curves, i.e., source-drain currents (I_{DS}) vs. source-gate voltage sweeps (V_{GS}). Transfer curves for increasing target concentrations diverged for dopamine- and glucose-aptamer-FETs vs. serotonin- and S1P-aptamer-FETs (Fig. 3, A to D). Dopamine and serotonin each have one positive charge at physiological pH. Transfer curve divergence for these molecules enables us to conclude that signal transduction mechanisms based exclusively on target charge, as has been proposed (23), are incorrect and preclude detecting neutral targets. The divergence of I-V curves also suggests different conformational changes upon target binding. For dopamine and glucose, transfer curves were consistent with aptamer reorientations occurring such that substantial portions of the negatively charged backbones moved closer to *n*-type semiconductor channels, increasing electrostatic repulsion of charge carriers (band bending) and decreasing transconductance, measured as target-related current responses (Fig. 3E). In contrast, we hypothesized that serotonin and S1P aptamers moved predominantly away from channel surfaces upon target capture increasing transconductance (Fig. 3F).

We used circular dichroism (CD) spectroscopy to gain additional insight (24, 25). For dopamine and serotonin, large changes in CD peak positions and relative intensities indicated shifts away from predominant duplex signals (maxima at ~280 nm) and formation of new target-induced structural motifs. A parallel (or mixed) G-quadruplex (maximum shifted to 260 nm) (26) was indicated for dopamine- (Fig. 4A) and an antiparallel G-quadruplex (maximum shifted to 290 nm) for serotonin-aptamer complexes (Fig. 4B). As

with fluorescence, FET, and SERS data, CD indicated selectivity of dopamine and serotonin aptamers for their targets vs. similarly structured countertargets (fig. S10, A and B). Although fluorescence, FET, and SERS findings specified target recognition for glucose and S1P aptamers, changes in CD spectra were not observed for these aptamers (fig. S10, C and D). Thus, for glucose and S1P aptamers, all major DNA domains, i.e., G-quartets, helices, and single-stranded regions, were formed prior to target binding and adaptive binding occurred through spatial rearrangement of existing secondary structures and companion ions (27).

We used Förster resonance energy transfer (FRET) to investigate changes in aptamer backbone distances during target-induced conformational changes. We identified FRET sensors for serotonin and glucose aptamers (table S6). For serotonin, the decrease in FRET (Fig. 4C, fig. S11A) was consistent with a substantial fraction of the longest loop in the G-quadruplex moving away from the semiconductor surface, and hence, with the upward shifts in FET transfer curves (Fig. 3B). For glucose, FRET results (Fig. 4D, fig. S11B) supported movement of the second stem in the aptamer toward the semiconductor surface, consistent with downward shifts in FET transfer curves (Fig. 3C). For the glucose aptamer, we increased the stem lengths for attachment to FET surfaces (Fig. 4C). Conductance responses decreased with additional base pairs (Fig. 4D), suggesting that recognition occurred further away from FETs as the attachment stems became longer. This strategy might be used to tune sensitivity ranges of sensor array elements thereby extending the ranges of arrays.

Together, all mechanistic findings are consistent with small-molecule-FETs enabling sensing under physiological conditions (Fig. 3, E and F) and without added aptamer labeling or surface chemistries (*cf.* ref. (28)). Importantly, because of the aptamer selection strategy, target-specific aptamer reorientations occur in close proximity to semiconductor surfaces, and in some cases, even in the absence of formation of new secondary structural motifs. General aptamer reorientation can be inferred from FET gate-voltage sweeps with additional FET mechanisms possibly contributing for specific sensors, e.g. band bending, and permittivity and mobility changes. Unlike large protein receptors (e.g., antibodies), highly selective, chemically synthesized, compact nucleic acid receptors identified through in vitro selection are amenable to affinity tuning (29, 30) and targeting of a wide variety of small (and large) molecules for electronic sensing (23).

Supplementary Material

Refer to Web version on PubMed Central for supplementary material.

Acknowledgments

The authors thank Prof. Donald Kuhn and Dr. Huajun Chen for resources and assistance. Current address for YSR is School of Intelligent Mechatronics Engineering, Sejong University, Seoul 05006, Republic of Korea.

Funding: This work was supported by NIH (DA045550, CA199849, GM104960), NSF (CCF1518715, 1509794, CMMI-1636136), CalBrain, NantWorks, Hewlett Packard, the Merkin Family Foundation, and the China Scholarship Council.

References and Notes:

1. Cui Y, Wei QQ, Park HK, Lieber CM, Nanowire Nanosensors for Highly Sensitive and Selective Detection of Biological and Chemical Species, Science 293, 1289–1292 (2001). [PubMed: 11509722]
2. Kim J et al., Fabrication of High-Performance Ultrathin In_2O_3 Film Field-Effect Transistors and Biosensors Using Chemical Lift-Off Lithography, ACS Nano 9, 4572–4582 (2015). [PubMed: 25798751]
3. Casal P et al., ImmunoFET Feasibility in Physiological Salt Environments, Philos. T. R. Soc. A 370, 2474–2488 (2012).
4. Vacic A et al., Determination of Molecular Configuration by Debye Length Modulation, J. Am. Chem. Soc 133, 13886–13889 (2011). [PubMed: 21815673]
5. Weiss PS, Trevor PL, Cardillo MJ, Gas Surface Interactions on InP Monitored by Changes in Substrate Electronic-Properties, J. Chem. Phys 90, 5146–5153 (1989).
6. Liao WS et al., Subtractive Patterning via Chemical Lift-Off Lithography, Science 337, 1517–1521 (2012). [PubMed: 22997333]
7. Shoorideh K, Chui CO, On the Origin of Enhanced Sensitivity in Nanoscale FET-Based Biosensors, Proc. Natl. Acad. Sci. U. S. A 111, 5111–5116 (2014). [PubMed: 24706861]
8. Landry MP et al., Single-Molecule Detection of Protein Efflux from Microorganisms Using Fluorescent Single-Walled Carbon Nanotube Sensor Arrays, Nat. Nanotechnol 12, 368–377 (2017) [PubMed: 28114298]
9. Yang KA, Pei R, Stojanovic MN, In Vitro Selection and Amplification Protocols for Isolation of Aptameric Sensors for Small Molecules, Methods 106, 58–65 (2016). [PubMed: 27155227]
10. Yang KA et al., Recognition and Sensing of Low-Epitope Targets via Ternary Complexes with Oligonucleotides and Synthetic Receptors, Nat. Chem 6, 1003–1008 (2014). [PubMed: 25343606]
11. Walsh R, DeRosa MC, Retention of Function in the DNA Homolog of the RNA Dopamine Aptamer, Biochem. Bioph. Res. Co 388, 732–735 (2009).
12. Altieri SC et al., Perinatal vs. Genetic Programming of Serotonin States Associated with Anxiety, Neuropsychopharmacology 40, 1456–1470 (2015). [PubMed: 25523893]
13. Nakatsuka N, Andrews AM, Differentiating Siblings: The Case of Dopamine and Norepinephrine, ACS Chem. Neurosci 8, 218–220 (2017). [PubMed: 28177214]
14. Yang H, Thompson AB, McIntosh BJ, Altieri SC, Andrews AM, Physiologically Relevant Changes in Serotonin Resolved by Fast Microdialysis, ACS Chem. Neurosci 4, 790–798 (2013). [PubMed: 23614776]
15. Alivisatos AP et al., Nanotools for Neuroscience and Brain Activity Mapping, ACS Nano 7, 1850–1866 (2013). [PubMed: 23514423]
16. Perez GI, Knudson CM, Leykin L, Korsmeyer SJ, Tilly JL, Apoptosis-Associated Signaling Pathways Are Required for Chemotherapy-Mediated Female Germ Cell Destruction, Nat. Med 3, 1228–1232 (1997). [PubMed: 9359697]
17. Rodeberg NT, Sandberg SG, Johnson JA, Phillips PEM, Wightman RM, Hitchhiker's Guide to Voltammetry: Acute and Chronic Electrodes for in Vivo Fast-Scan Cyclic Voltammetry, ACS Chem. Neurosci 8, 221–234 (2017). [PubMed: 28127962]
18. Ke C, Destecroix H, Crump MP, Davis AP, A Simple and Accessible Synthetic Lectin for Glucose Recognition and Sensing, Nat. Chem 4, 718–723 (2012). [PubMed: 22914192]
19. Purschke WG et al., Identification and Characterization of a Mirror-Image Oligonucleotide That Binds and Neutralizes Sphingosine 1-Phosphate, a Central Mediator of Angiogenesis, Biochem. J 462, 153–162 (2014). [PubMed: 24832383]
20. Masango SS et al., High-Resolution Distance Dependence Study of Surface-Enhanced Raman Scattering Enabled by Atomic Layer Deposition, Nano Lett. 16, 4251–4259 (2016). [PubMed: 27243108]
21. Angoa-Perez M et al., Mice Genetically Depleted of Brain Serotonin Do Not Display a Depression-Like Behavioral Phenotype, ACS Chem. Neurosci 5, 908–919 (2014). [PubMed: 25089765]

22. Chen XN, Margolis KJ, Gershon MD, Schwartz GJ, Sze JY, Reduced Serotonin Reuptake Transporter (SERT) Function Causes Insulin Resistance and Hepatic Steatosis Independent of Food Intake, PLoS One 7, (2012).
23. Nakatsuka N, Weiss PS, Andrews AM, Towards Electronic Biosensing in Vivo: Aptamer Field-Effect Transistors, Chem. Rev., in preparation (2018).
24. Liu W et al., Kinetics and Mechanism of Conformational Changes in a G-Quadruplex of Thrombin-Binding Aptamer Induced by Pb^{2+}, J. Phys. Chem. B 115, 13051–13056 (2011). [PubMed: 21950308]
25. Nagatoishi S, Tanaka Y, Tsumoto K, Circular Dichroism Spectra Demonstrate Formation of the Thrombin-Binding DNA Aptamer G-Quadruplex under Stabilizing-Cation-Deficient Conditions, Biochem. Bioph. Res. Co 352, 812–817 (2007).
26. Kypr J, Kejnovská I, Renčiuk D, Vorlíčková M, Circular Dichroism and Conformational Polymorphism of DNA, Nucleic Acids Res. 37, 1713–1725 (2009). [PubMed: 19190094]
27. Nagai Y et al., An Electrochemically Controlled Microcantilever Biosensor, Langmuir 29, 9951–9957 (2013). [PubMed: 23841706]
28. Gao N et al., Specific Detection of Biomolecules in Physiological Solutions Using Graphene Transistor Biosensors, Proc. Natl. Acad. Sci. U. S. A 113, 14633–14638 (2016). [PubMed: 27930344]
29. Ricci F, Valee-Belisle A, Simon AJ, Porchetta A, Plaxco KW, Using Nature's "Tricks" to Rationally Tune the Binding Properties of Biomolecular Receptors, Acc. Chem. Res 49, 1884–1892 (2016). [PubMed: 27564548]
30. Armstrong RE, Strouse GF, Rationally Manipulating Aptamer Binding Affinities in a Stem-Loop Molecular Beacon, Bioconjugate Chem. 25, 1769–1776 (2014).
31. Velez TE et al., Systematic Evaluation of the Dependence of Deoxyribozyme Catalysis on Random Region Length, ACS Comb. Sci 14, 680–687 (2012). [PubMed: 23088677]
32. Pobanz K, Lupták A, Improving the Odds: Influence of Starting Pools on in Vitro Selection Outcomes, Methods 106, 14–20 (2016). [PubMed: 27109058]
33. McKeague M et al., Analysis of in Vitro Aptamer Selection Parameters, J. Mol. Evol 81, 150–161 (2015). [PubMed: 26530075]
34. Thiel K, Oligo Oligarchy - The Surprisingly Small World of Aptamers, Nat. Biotechnol 22, 649–651 (2004). [PubMed: 15175673]
35. Hu J, Easley CJ, A Simple and Rapid Approach for Measurement of Dissociation Constants of DNA Aptamers against Proteins and Small Molecules via Automated Microchip Electrophoresis, Analyst 136, 3461–3468 (2011). [PubMed: 21293790]
36. Hwang YH et al., An 'Aqueous Route' for the Fabrication of Low-Temperature-Processable Oxide Flexible Transparent Thin-Film Transistors on Plastic Substrates, NPG Asia Mater. 5, (2013).
37. Chen H et al., Quasi-Two-Dimensional Metal Oxide Semiconductors Based Ultrasensitive Potentiometric Biosensors, ACS Nano 11, 4710–4718 (2017). [PubMed: 28430412]
38. Rim YS et al., Printable Ultrathin Metal Oxide Semiconductor-Based Conformal Biosensors, ACS Nano 9, 12174–12181 (2015). [PubMed: 26498319]
39. Tang T et al., Complementary Response of In_2O_3 Nanowires and Carbon Nanotubes to Low-Density Lipoprotein Chemical Gating, Appl. Phys. Lett 86, (2005).
40. Curreli M et al., Selective Functionalization of In_2O_3 Nanowire Mat Devices for Biosensing Applications, J. Am. Chem. Soc 127, 6922–6923 (2005). [PubMed: 15884914]
41. Rim YS et al., Boost up Mobility of Solution-Processed Metal Oxide Thin-Film Transistors via Confining Structure on Electron Pathways, Adv. Mater 26, 4273–4278 (2014). [PubMed: 24740439]
42. Ishikawa FN et al., A Calibration Method for Nanowire Biosensors to Suppress Device-to-Device Variation, ACS Nano 3, 3969–3976 (2009). [PubMed: 19921812]
43. Bengel D et al., Altered Brain Serotonin Homeostasis and Locomotor Insensitivity to 3,4-Methylenedioxymethamphetamine ("Ecstasy") in Serotonin Transporter-Deficient Mice, Mol. Pharmacol 53, 649–655 (1998). [PubMed: 9547354]

44. Hait G et al., Alteration of Glucose and Insulin Metabolism in Congenital Heart-Disease, Circulation 46, 333–346 (1972). [PubMed: 5046027]
45. Moskovits M, Surface-Enhanced Raman Spectroscopy: A Brief Retrospective, J. Raman Spectrosc 36, 485–496 (2005).
46. Doering WE, Nie SM, Single-Molecule and Single-Nanoparticle Sers: Examining the Roles of Surface Active Sites and Chemical Enhancement, J. Phys. Chem. B 106, 311–317 (2002).
47. Le Ru EC, Etchegoin PG, Single-Molecule Surface-Enhanced Raman Spectroscopy, Annu. Rev. Phys. Chem 63, 65–87 (2012). [PubMed: 22224704]
48. Otto C, van den Tweel TJJ, de Mul FFM, Greve J, Surface-Enhanced Raman-Spectroscopy of DNA Bases, J. Raman Spectrosc 17, 289–298 (1986).
49. Pagba CV, Lane SM, Cho HS, Wachsmann-Hogiu S, Direct Detection of Aptamer-Thrombin Binding via Surface-Enhanced Raman Spectroscopy, J. Biomed. Opt 15, (2010).
50. Barhoumi A, Zhang D, Halas NJ, Correlation of Molecular Orientation and Packing Density in a dsDNA Self-Assembled Monolayer Observable with Surface-Enhanced-Raman Spectroscopy, J. Am. Chem. Soc 130, 14040–14041 (2008). [PubMed: 18834128]
51. Camden JP, Dieringer JA, Zhao J, Van Duyne RP, Controlled Plasmonic Nanostructures for Surface-Enhanced Spectroscopy and Sensing, Acc. Chem. Res 41, 1653–1661 (2008). [PubMed: 18630932]
52. Lal S et al., Tailoring Plasmonic Substrates for Surface Enhanced Spectroscopies, Chem. Soc. Rev 37, 898–911 (2008). [PubMed: 18443675]
53. Yunker PJ, Still T, Lohr MA, Yodh AG, Suppression of the Coffee-Ring Effect by Shape-Dependent Capillary Interactions, Nature 476, 308–311 (2011). [PubMed: 21850105]
54. Neumann O et al., Direct Optical Detection of Aptamer Conformational Changes Induced by Target Molecules, Anal. Chem 81, 10002–10006 (2009). [PubMed: 19928834]
55. Willets KA, Van Duyne RP, Localized Surface Plasmon Resonance Spectroscopy and Sensing, Annu Rev Phys Chem 58, 267–297 (2007). [PubMed: 17067281]

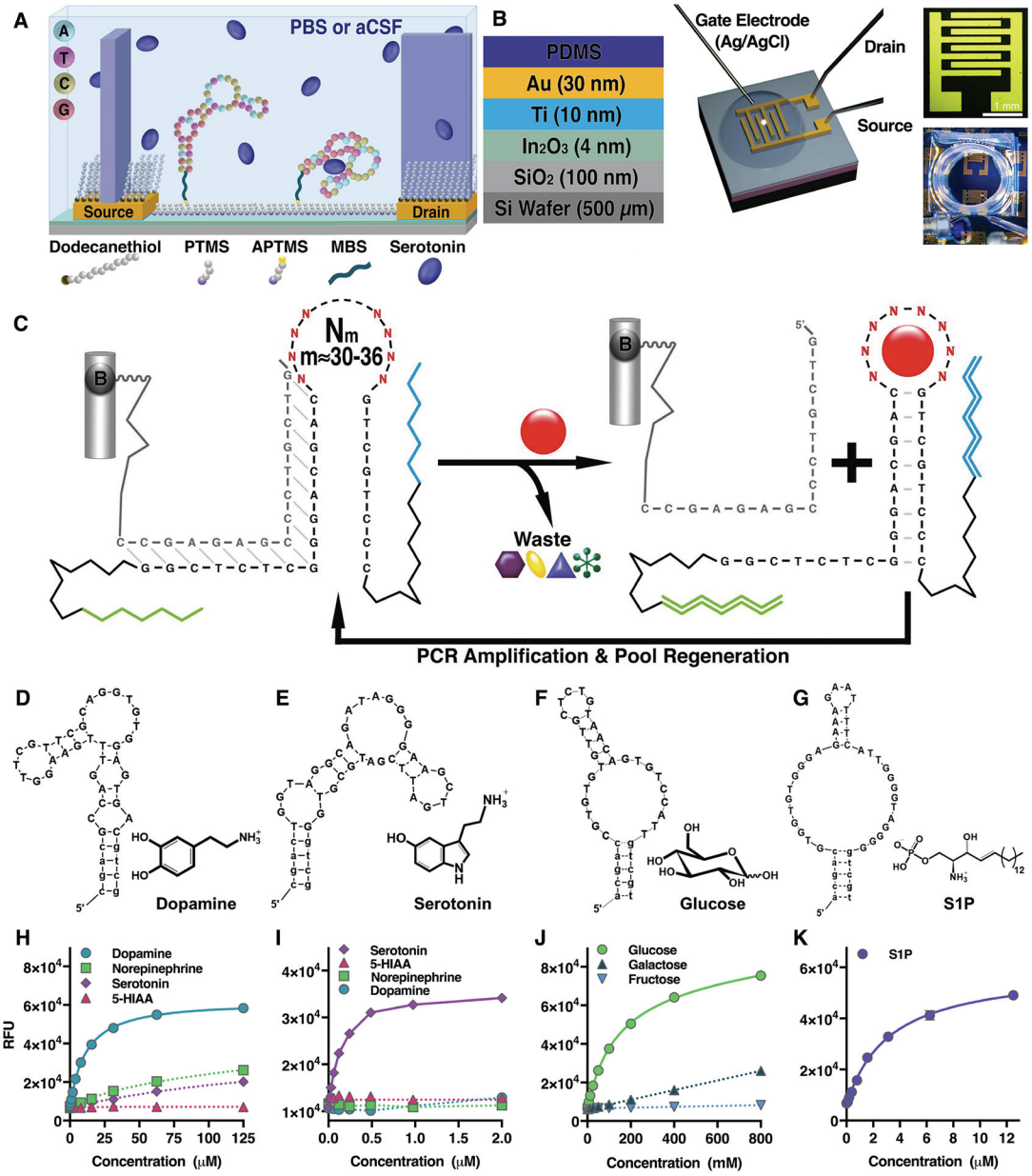

Fig. 1. Isolation of stem-loop aptamer receptors.

(**A**) Schematic of field-effect transistor surface chemistry. (**B**) Layer-by-layer composition of FETs, FET microscope image, and photograph of experimental setup. (**C**) Oligonucleotide libraries (N_m, with random regions m from 30 to 36 nucleotides, flanked by constant regions and oligonucleotide primer regions for PCR amplification) were attached to agarose-streptavidin columns *via* biotinylated (B) complementary sequences. Exposure to targets (red sphere) causes elution of aptamers in which stems are stabilized. These sequences are preferentially amplified. Exposure to countertargets (alternate shapes) eliminates cross-reactive sequences. Aptamers for **(D)** dopamine (K_d=150 nM), (**E**) serotonin (K_d=30 nM), (**F**) glucose (K_d=10 mM), and **(G)** S1P (K_d=190 nM) were isolated. Solution-phase SELEX selected for aptamers that were directly converted to sensors. The complementary

oligonucleotide was labeled with a quencher instead of biotin, while the aptamer was labeled with a fluorophore, leading to adaptive binding sensors with responses shown in (**H to K**). Fluorescence responses indicate selectivities of dopamine, serotonin, and glucose aptamers in the presence of specific vs. nonspecific targets. Fluorescence-concentration curves were the result of N=3 measurements with SEMs too small to be visualized in the graphs shown.

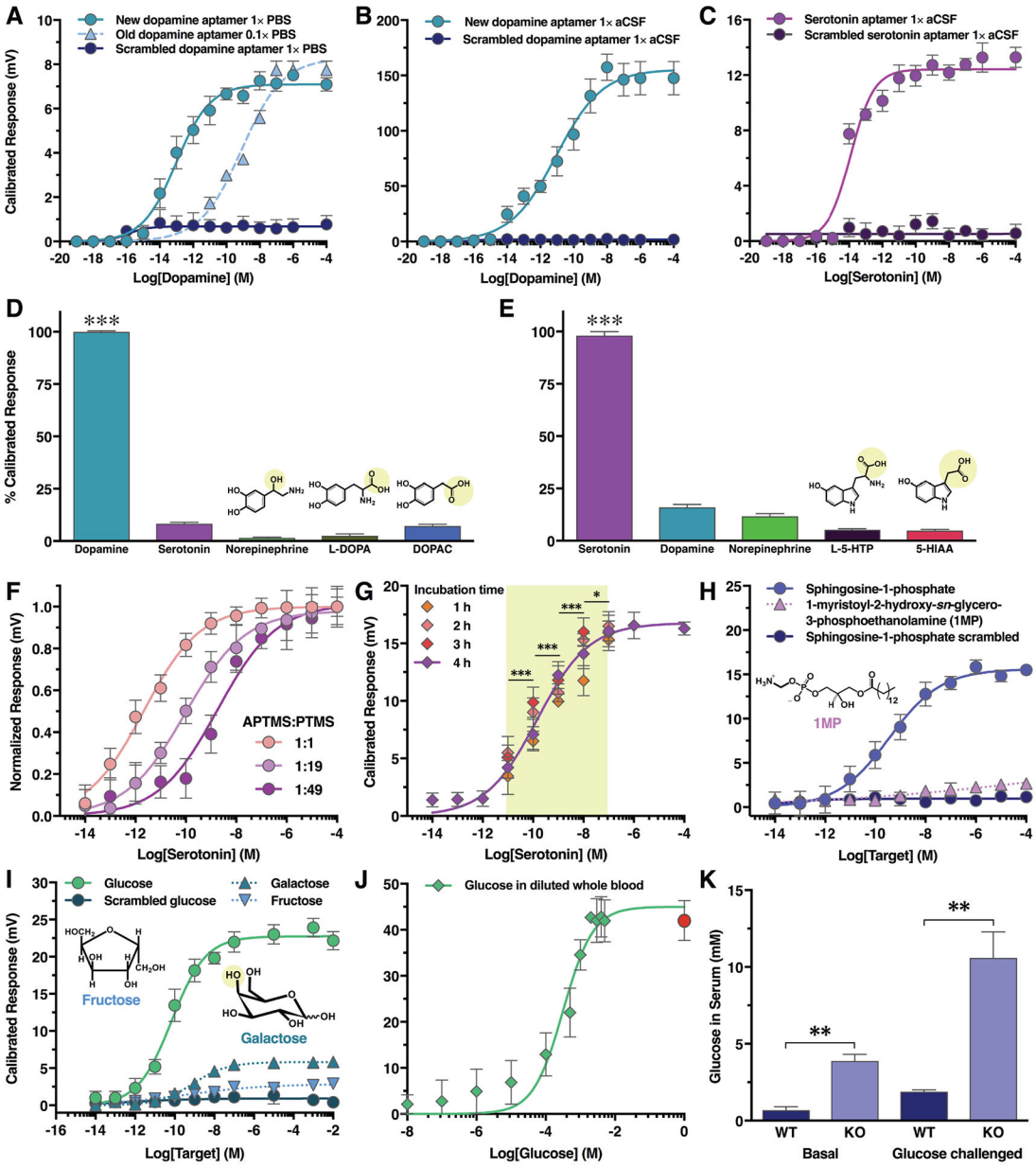

Fig. 2. Electronic small-molecule detection using aptamer-functionalized field-effect transistor (FET) sensors

(**A**) Responses of FET sensors functionalized with the new dopamine aptamer (K_d=150 nM, full strength phosphate-buffered saline (1**X** PBS)) or its scrambled sequence, compared to FET responses with a previously reported dopamine aptamer (K_d=1 μM, 0.1**X** PBS) (2). (**B**) New dopamine aptamer and scrambled aptamer-FET responses to dopamine in artificial cerebrospinal fluid (1**X** aCSF). (**C**) For serotonin-aptamer-FETs, serotonin in 1**X** aCSF led to concentration-dependent responses, while scrambled serotonin sequences showed negligible responses. (**D**) New dopamine-aptamer-FET responses to 100 μM norepinephrine, serotonin, *L*-3,4-dihydroxyphenylalanine (*L*-DOPA), and 3,4-dihydroxyphenylacetic acid (DOPAC) were negligible compared to dopamine (10 nM). (**E**) Serotonin-aptamer-FET responses to 100 μM dopamine, norepinephrine, 5-hydroxytryptophan (L-5-HTP), or 5-

hydroxyindoleacetic acid (5-HIAA) were negligible compared to serotonin (10 nM). (**F**) Serotonin aptamer-FET sensitivities were shifted by altering ratios of amine-:methyl-terminated silanes for surface tethering. (**G**) Serotonin-aptamer-FETs after 1–4 h incubation in serotonin-free brain tissue followed by addition of serotonin exhibited reproducible responses with differentiable physiological concentrations. (**H**) Sphingosine-1-phosphate (S1P) aptamer-FETs showed concentration-dependent responses to S1P but not a phospholipid with similar epitopes or a scrambled sequence in 1x HEPES. (**I**) Glucose sensing in 1**X** Ringer's buffer. Responses of glucose-aptamer-FETs were minimal or negligible for galactose, fructose, and a scrambled sequence. (**J**) Glucose aptamer-FET responses in mouse whole blood diluted in Ringer's to construct a concentration curve. The red circle represents response in undiluted whole blood. (**K**) Glucose aptamer-FETs enabled differentiation of hyperglycemia in serotonin transporter deficient (KO) mice *vs.* wildtype (WT) mice by measuring glucose levels in diluted serum under basal and glucose challenged conditions. All calibrated responses were at gate voltage V_G = 100 mV. Error bars are +/− SEM with $N = 6$ (**A–C, H, I**) or $N = 3$ samples per group (**D–G, J, K**).

*** $P < 0.001$ vs. countertargets;

** $P < 0.01$ KO vs. WT.

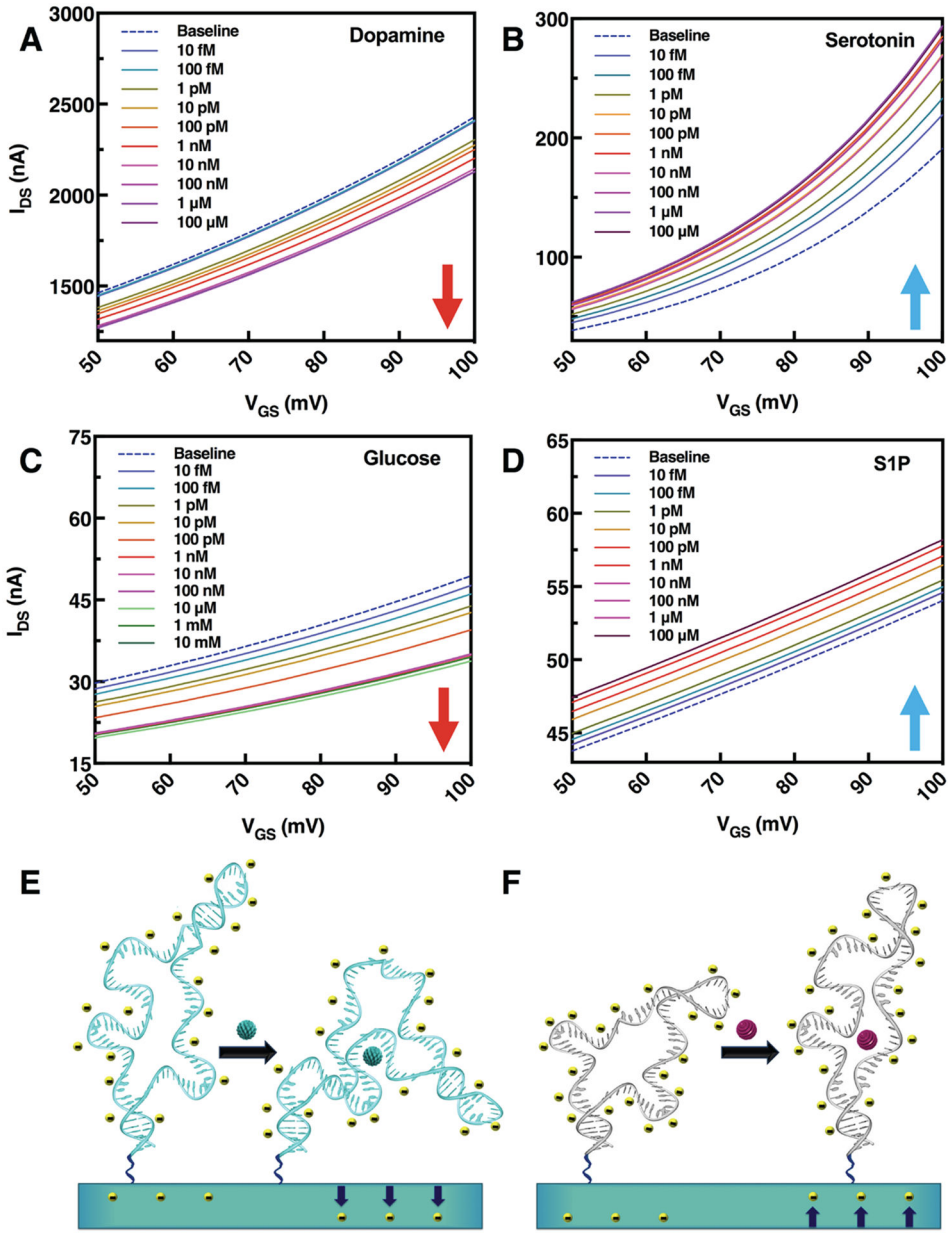

Fig. 3. Aptamer-functionalized field-effect transistor (FET) mechanisms.

(**A**) Exposure of dopamine-aptamer-FETs to dopamine (artificial cerebrospinal fluid; 1x aCSF)) led to concentration-dependent reductions in source-drain currents. (**B**) For serotonin-aptamer-FETs, increasing concentrations of serotonin (1x aCSF) produced increases in source-drain currents. (**C**) Exposure of glucose aptamer-FETs to glucose (1x Ringer's) led to reductions in source-drain currents. (**D**) The S1P aptamer-FET transfer curves (1x HEPES) increased in response to target concentrations. Transfer curves shown are representative of N=6 individual measurements. (**E,F**) Hypothesized mechanism of stem-loop aptamer target-induced reorientations in close proximity to semiconductor channels and within or near the Debye length. In (**E**), aptamers reorient closer to FETs to deplete channels electrostatically (e.g., dopamine, glucose). In (**F**), aptamer stem-loops

reorient *away* from semiconductor channels increasing transconductance (e.g., serotonin, S1P). Schematics are idealized and do not reflect individual aptamer secondary structural motifs.

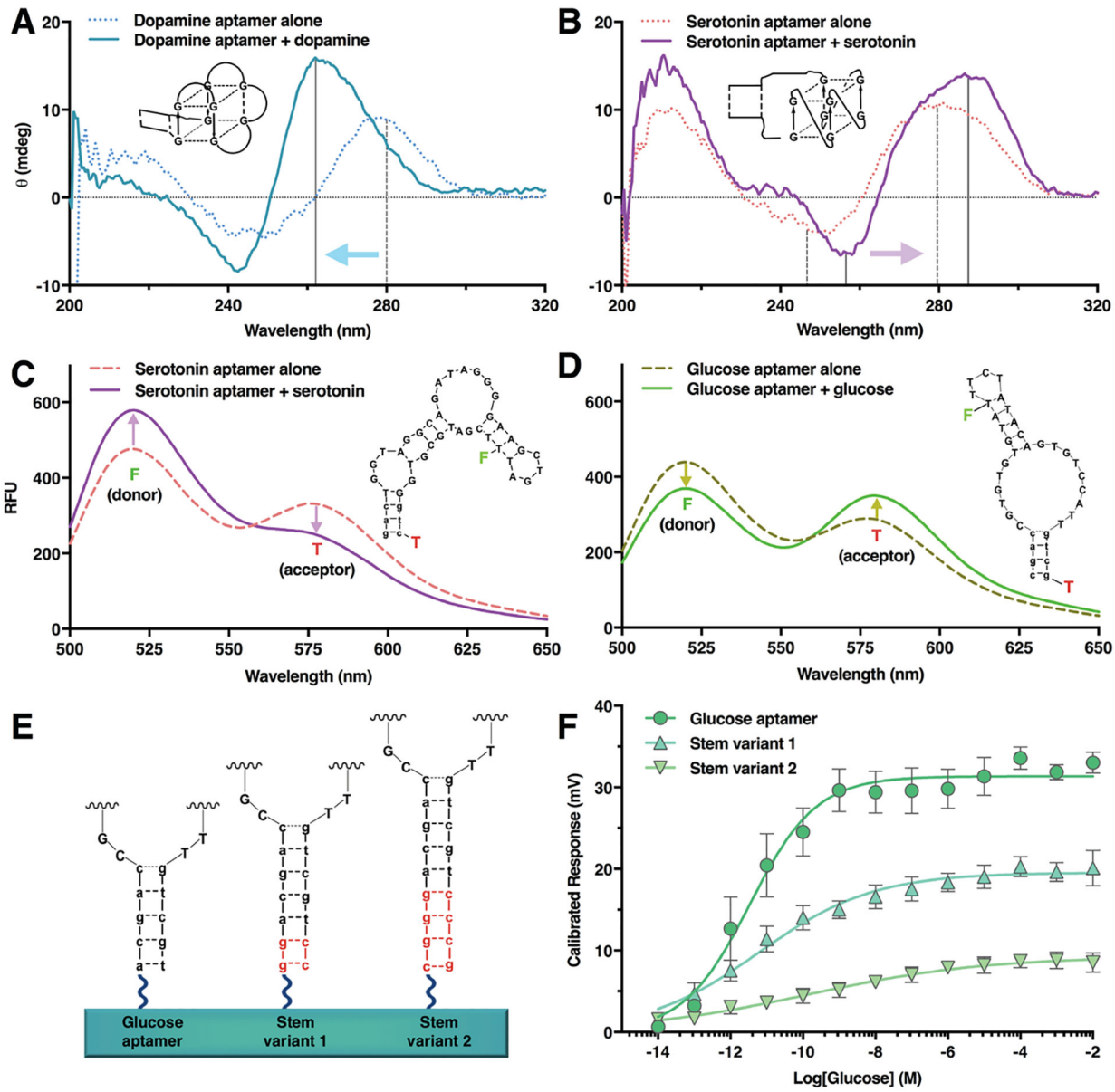

Fig. 4. Changes in aptamer secondary structures upon adaptive binding to small-molecule targets.

(**A**) Circular dichroism spectroscopy of the dopamine aptamer upon target capture showed significant shifts indicating formation of a compact parallel G-quadruplex (1x aCSF). (**B**) By contrast, the serotonin aptamer showed a shift in peak positions indicating formation of an antiparallel G-quadruplex. Förster resonance energy transfer (FRET) between donor-, fluorescein (F), excited at 470 nm, and acceptor-, 5-carboxytetramethylrhodamine (T), labeled aptamers was monitored before and after target incubation. (**C**) For serotonin aptamers, donor fluorescence increased while acceptor emission decreased upon serotonin incubation suggesting that fluorophores move further away from each other upon target exposure. (**D**) Conversely, for glucose aptamers, the emission spectra for the acceptor increased while donor fluorescence decreased upon glucose exposure indicative of acceptor

moving closer to donor enabling increased energy transfer. Stem-loop movement directions indicated by FRET for glucose vs. serotonin aptamers are consistent with their divergent FET transfer curve directions in Figure 3. (**E**) For glucose-aptamer-FETs with rigid double-stranded attachment stems (left), increasing distances from semiconductor surfaces by increasing the stem lengths (stem variants; right) resulted in (**F**) length-associated decreases in FET calibrated responses (1x Ringer's solution). Spectra shown in **A–D** are representative of N=2 samples per condition; error bars in **F** are +/− SEMs with N=3 samples per group.